Freestream Turbulence Measurements in Icing Conditions

C.M. Henze[+], M.B. Bragg[*], H.S. Kim[#]
University of Illinois at Urbana-Champaign

Abstract

Current understanding of the ice accretion process is based largely on icing wind tunnel tests. Turbulent fluctuations in the freestream, which are different in the wind tunnel than in flight, have been identified as having potentially important effects on the results of tests performed in icing tunnels. The turbulence intensity level in icing tunnels with the spray cloud turned off had been previously measured and found to be quite high due to the lack of turbulence reducing screens, and to the presence of the spray system. However, the turbulence intensity level in the presence of the spray cloud had not been measured. In this study, a method for making such measurements was developed and used to study the effects of the spray cloud on the turbulence level in the NASA Lewis Icing Research Tunnel (IRT). Turbulent velocity fluctuations were measured using hot-wire sensors. Droplets striking the wire resulted in distinct spikes in the hot-wire voltage which were removed using a digital acceleration threshold filter. The remaining data were used to calculate the turbulence intensity. Using this method, the turbulence intensity level in the IRT was found to be highly dependent on nozzle air pressure, while other factors such as nozzle water pressure, droplet size, and cloud liquid water content had little effect.

Introduction

Wind tunnel testing has played and will continue to play an important role in our attempt to understand the physical processes behind ice accretion and its effects on aircraft performance. While wind tunnel testing is an invaluable tool, there will always be important differences between the wind tunnel environment and that which an aircraft sees in flight. For this reason, caution should always be taken in applying test results, and attempts should be made to identify these differences and assess their influence on test results whenever possible. One problem of particular importance, which has long been recognized, is the turbulent fluctuations in wind tunnel flows which are often considerably larger than those in the atmosphere. In 1920 the British Aeronautical Research Committee acknowledged the importance of tunnel turbulence when they proposed that, in an attempt to standardize wind tunnel testing, a series of identical tests be performed in wind tunnel facilities throughout the world.[1] The influence of freestream turbulence is of particular importance in the study of aircraft icing since turbulence levels in flight are generally quite low while the turbulence intensity in tunnels used for icing research is inherently high. This is due to the lack of anti-turbulence screens, and to the turbulence generated by the spray apparatus. Gonsalez[2] has measured turbulence levels in the NASA Lewis Icing Research Tunnel (IRT) ranging from approximately 0.5% at 50 mph to 1.5% at 325 mph. With the nozzle spray air (no water) operating, he saw even higher turbulence levels which varied from around 0.8% at moderate speeds up to approximately 2% at a speed of 350 mph. The turbulence measurements taken by Gonsalez are shown as a function of velocity in Fig. 1. In similar measurements, Poinsatte[3] found turbulence levels in the IRT ranging from 0.5-0.7% over a range of 70 to 210 mph without the spray nozzle air operating. He also measured higher levels with the nozzle air (no water) on, but these values weren't reported due to concerns about temperature fluctuations which will be discussed later. In contrast, taking hot-wire measurements in flight, Poinsatte measured turbulence intensity levels of less than 0.1% in clear air.

Importance of Freestream Turbulence in Ice Accretion Physics

The role of freestream turbulence in the ice accretion process is not well understood. While there are several possible ways in which increased velocity fluctuations

---

[+] Graduate Research Assistant, Dept. of Aeronautical and Astronautical Engineering.
Currently Associate Engineer, Hamilton Standard, Windsor Locks, Connecticut, Member AIAA.
[*] Professor, Dept. of Aeronautical and Astronautical Engineering, Associate Fellow AIAA.
[#] Graduate Research Associate, Dept. of Aeronautical and Astronautical Engineering, Member AIAA.

could affect the accretion of ice, it seems likely that enhancement of heat transfer in the region of ice growth and over the ice shape itself would play the most important role.

It is well accepted that increases in turbulence intensity can affect the structure of the boundary layer, in particular by moving the location of boundary layer transition toward the leading edge.[4,5] Changes in the boundary layer structure are likely to affect ice accretion since heat transfer is increased in the presence of transitional and turbulent boundary layers. Kuethe and Chow[4] state that the turbulence level in the atmosphere is essentially zero as far as its effect on boundary layer transition is concerned. Green[6] calculated that a turbulence level of just 0.2% results in a 1% increase in skin friction coefficient, and a decrease of 0.005 in boundary layer shape factor. Bragg et al.[7] found that when they increased the turbulence intensity level to 0.95% to simulate the high levels seen in icing tunnels, no truly laminar flow was observed on the model. The flow was already transitional in the leading edge region. In studying the effects of freestream turbulence on heat transfer from a flat plate with a pressure gradient, Junkhan and Serovy[8] attributed the increase in heat transfer which they observed with increased turbulence levels of 1.8 to 5% to the fact that the boundary layer was no longer laminar but had become transitional.

In studies connecting the change in boundary layer structure to increases in heat transfer, it has been noted that when no pressure gradient was present, increased freestream turbulence had a negligible effect on heat transfer as long as the boundary layer remained laminar.[8,9] However, for a fully turbulent boundary layer, Blair observed an increase in heat transfer on a zero pressure gradient flat plate of up to 20% when turbulence intensity was increased from 0.25 to 7%. This suggests that increased freestream turbulence intensity can increase heat transfer through turbulent, and possibly transitional, boundary layers. With turbulence intensity increased to approximately 2.4% Van Fossen and Simoneau[10] found a 30% increase in heat transfer from a cylinder. In an earlier study, Van Fossen et al.[11] found similar increases in heat transfer on models of ice shapes based on actual ice accretions measured in the IRT.

Of particular interest to the present study are the works of Gelder and Lewis[12] and Poinsattte[3] in which comparisons of heat transfer on an airfoil in flight and in the IRT have been made. Gelder and Lewis found an increase in heat transfer of as much as 30% in the IRT. Poinsatte's more recent investigation of heat transfer from an NACA 0012 found a maximum heat transfer increase in the IRT of 10% over heat transfer in flight. He observed a 2-3% increase over the flight condition near the leading edge of the model at 0% angle of attack and $Re = 1.2x10^6$. With the nozzle air on, a 3-5% increase was seen. Further back on the airfoil, the increase in heat transfer was even larger, and larger increases in heat transfer were also seen with increasing Reynold's number. These studies all indicate that increased turbulence has a strong effect on heat transfer, and it is logical that such increased heat transfer would affect ice accretion. It is thus important to characterize the turbulence level in flight icing conditions and icing wind tunnels so that we can begin to assess the effects of turbulence intensity on icing tunnel results.

Hot-wire Anemometry in Two-Phase Flows

While hot-wire anemometry is the most popular method of measuring turbulent fluctuations, the icing wind tunnel environment presents a particular problem in the use of this method. The presence of the water droplets has a significant effect on the hot-wire signal. In order to successfully measure turbulence in these conditions, a method must be developed for separating the droplet strikes from the turbulent fluctuations in the free stream. Numerous researchers have addressed this problem, and more generally the problem of phase discrimination in any two-phase flow.

The use of hot films and hot wires for measuring turbulence in rain storms was addressed by Merceret.[13,14] By dropping rain drop size water droplets, 0.3 - 0.5 cm, on hot wires and hot films in a plexiglass tube with no flow present, he was able to examine the signal returned when a droplet hit the anemometer sensor. He noted a high spike in the signal due to the increased heat transfer to the water droplet, and referenced work by other researchers where a similar spike had been observed in work with aerosol droplets. Similar data were taken in rain storms with winds less than 20 meters per second from a tower on top of the laboratory.[13,14] In these conditions, Merceret observed a clearly distinguishable droplet strike signal from a wedge shaped hot film, but found that hot wires were not useable in these conditions because the signal from large and small droplets could not be clearly differentiated from the turbulence signal. Goldschmidt, and Householder[15] however, found hot-wire sensors suitable for use as particle concentration and size samplers as well as turbulence sensors.

Hetsroni, Cutler, and Sokolov[16] experimented with the use of hot wires in particle contaminated flow and described the method by which their data were analyzed. A threshold voltage was set such that any voltage above it was considered to represent a droplet strike, and "clipper and pickoff" circuits were employed. The "pickoff" circuit passed only signals above the voltage threshold which were then fed to instruments which counted the number of droplets impinging during a set period of time. The "clipper" circuit passed all voltages below the threshold to DC and true rms voltmeters for measuring time-averaged velocity and turbulence intensity. Because of the remaining "stumps" of the droplet strikes, corrections had to be made to these measurements.

Hetsroni, and Sokolov[17] made some important observations when they applied this method to two-phase turbulent jet flow. Droplets 13 microns in diameter were injected into the flow prior to exiting a 25 mm diameter nozzle. The exit velocity was 50 m/sec (~112 mph). This study is of particular interest because this drop size and velocity are within the capabilities of the IRT. Measurements of time-averaged and fluctuating velocities along with droplet flux were taken at several locations downstream of the nozzle. They noted that the droplets were almost immediately swept off the wire and the signal returned quickly to the initial heat transfer level. They also observed that some small droplets caused signals which were only slightly greater than the turbulent signals and thus fell under the threshold voltage. However, they assumed that in general the signals due to droplet strikes were much higher than those due to turbulent fluctuations.

Much of the more recent work concerning the use of thermal anemometry in two-phase flows has involved "bubbly flows" of gas bubbles in a liquid flow. While this is a considerably different application, many of the phase discrimination techniques used are applicable in air flows containing water droplets. The relatively large size and slow speed of the bubbles in these flows allows for careful analysis of the low heat transfer region indicative of a bubble passing the sensor. Such analyses, in which the different regions of the bubble and even the approach of the bubble are detected, is outlined in detail in Bruun[18], Liu and Bankoff[19] and Farrar et al.[20] The most important thing to be noted from this work is that these analyses apply threshold criteria not only to the voltage signal or the resultant velocity, but also to the slope of the signal or the acceleration. In an observation similar to that made by Hetsroni and Sokolov,[17] Farrar et al.[20] noted that, "some partial bubble hits or small bubbles," were not detected by a simple voltage threshold. However, they noted that the slope of the voltage at the passing of the bubble was generally an order of magnitude higher than the slopes found in the freestream data. When a threshold filter was applied to the slope, rather than the voltage, the detection of most of these difficult to detect impingements was possible.

A slope threshold method was applied to air flow containing liquid droplets by Ritsch and Davidson.[21] In this work, hot-film measurements were taken in 0.6 m/s duct flow containing 2 μm atomized oleic acid particles. The average slope between data points was calculated, and when the slope between any two points exceeded 6 times the average, those points were considered to be in the liquid phase. When the time between particle impingements was large compared to the duration of the event itself, the signals within the spike were replaced by the last value prior to exceeding the slope threshold. However, it was noted that it was better to remove the particle spikes and reduce the number of data points in cases where the spikes compose a larger portion of the data set. It was also noted that a high data rate, 20 kHz was used by Ritsch and Davidson,[21] was necessary to detect the rapid phase changes.

These studies suggest that thermal anemometry can be used as a practical means of measuring turbulent fluctuations in atmospheric and icing tunnel cloud conditions provided an effective method is used to discriminate the water droplet strikes from the freestream turbulent fluctuations. It is apparent that applying only an amplitude threshold to the digitized signal would likely not be sufficient in detecting small droplets or partial droplet strikes. Several researchers have found that applying a threshold filter to the slope of the signal is more effective in detecting these smaller amplitude signals.

Experimental Objectives and Approach

The previous review of literature has shown that increased turbulent fluctuations affect the boundary layer development causing early transition. These changes in the structure of the boundary layer not only affect general performance measurements such as lift and drag, but have been shown to cause increased heat transfer. This increased heat transfer is likely to affect ice accretion. For these reasons it is important to characterize the turbulence level in icing tunnels. However, the measurement of turbulence intensity using hot-wire anemometry in icing tunnels is complicated by two factors. The first of these is the droplet strike fluctuations in the anemometer signal which will have to be removed from the data if accurate turbulence measurements are to be made. Second is the concern that the heated nozzle air may cause temperature fluctuations which will be misinterpreted by the hot wire as velocity fluctuations.

Thus, there are three specific objectives of the research reported here:

- Develop an effective method for measuring turbulence intensity in icing tunnel cloud conditions.
- Use the method to measure the turbulence intensity level in the spray cloud of the NASA Lewis Icing Research Tunnel at various cloud conditions.
- Determine the effects of temperature fluctuations due to heated nozzle air on these turbulence intensity measurements.

These objectives were investigated experimentally in three wind tunnel tests. It was initially hoped that the hot-wire sensor could be shielded from the majority of the droplets in the flow by placing it between the boundary layer and the droplet trajectories above an airfoil at angle of attack as illustrated in Fig. 2. The first of the three wind tunnel tests was performed at the University of Illinois, and was designed to assess the effects of the presence of the model on the turbulence intensity readings.

Two tests were performed in the NASA Lewis Icing Research Tunnel. In the first test, the probe was shielded by an airfoil as previously described. The primary goal of this test was to acquire data in support of developing the

turbulence measurement technique for use in cloud conditions. In the second IRT test, the possible temperature fluctuations were addressed by acquiring data both with and without the nozzle air heated. No model was used in this test in order to evaluate the need for shielding the sensor.

Experimental Apparatus and Methods

A brief description of the experimental apparatus and methods employed in the tests will be given here. For a more thorough description of the experimental facilities and apparatus as well as the experimental method, see Henze.[22]

Data Acquisition and Hot-wire Anemometry

The hot-wire anemometry system used was a TSI Incorporated IFA100. The hot-wire probes chosen were TSI model 1210 general purpose probes. The 1.27 mm long wires on these probes were platinum coated tungsten with diameters of 3.8 or 5.1 microns. The hot-wire sensors were calibrated in a small wind tunnel at the University of Illinois. A Pentium PC with a National Instruments AT-MIO-16x analog to digital data-acquisition board was used to acquire data from the anemometer. Through the use of signal conditioners, both DC and high-pass filtered signals were recorded.

Data Reduction Methods

Prior to being converted to velocities, the hot-wire voltages were corrected for the difference between the ambient temperature at the time of data acquisition, and the ambient temperature at which the wire was calibrated. The corrected voltage, E_{tc}, as given in the anemometer instruction manual[23] was:

$$E_{tc} = E\sqrt{\frac{(T_w - T_{cal})}{(T_w - T_{amb})}} \qquad (1)$$

where E is the anemometer output voltage, T_w is the hot-wire operating temperature, and T_{cal} and T_{amb} are the ambient temperatures at calibration and data acquisition, respectively. Velocities were then calculated from these temperature corrected voltages by means of a calibration polynomial which was derived for each wire from the calibration data.

In a similar manner to the temperature correction, the temperature-corrected velocities were corrected for differences in the air density at calibration and acquisition. The temperature and density corrected velocity, U_{tdc}, is given by eq. (2).[24]

$$U_{tdc} = U_{tc}\left(\frac{P_{cal}\,T_{amb}}{P_{amb}\,T_{cal}}\right) \qquad (2)$$

U_{tc} is the temperature corrected velocity found from the temperature corrected voltage. P_{cal} and P_{amb} are the calibration and acquisition ambient pressures.

After all of the temperature and density corrected values were found, mean values of the original and temperature corrected voltages, and the temperature and density corrected velocities were calculated. The standard deviation in the temperature corrected voltage, and the final velocity were calculated using the following equation:

$$x'_{rms} = \left(\frac{1}{T}\int_0^T x'^2\,dt\right)^{1/2} \qquad (3)$$

In eq. (3), x′ is the fluctuation of any quantity from its mean, and T is the total time. The turbulence intensity, defined as the standard deviation of the velocity, u'_{rms}, normalized by the mean velocity, in this case U_{test}, and expressed as a percentage was then calculated using the following equation:

$$TI = \frac{u'_{rms}}{U_{test}} \times 100 \qquad (4)$$

It is important to note that for data which had droplets removed, the integration in (3) was only performed between points which were originally adjacent to each other in the time trace, and not between points separated by a droplet strike. The following equation summarizes the turbulence intensity calculation for data which had droplet strikes removed.

$$TI_{filt} = \left(\frac{1}{T_{filt}}\sum_{i=1}^{m}\sum_{j=1}^{n_i-1}\left(\frac{u'^2_{j+1} + u'^2_j}{2}\right)t\right)^{1/2} \qquad (5)$$

In this equation, T_{filt} is the total time remaining after droplets have been removed, m is the number of segments of data which don't contain a droplet, n_i is the number of data points in the i^{th} such segment, u'_j is the deviation of the j^{th} voltage from the mean, and Δt is the time between data points.

Model Shielding Effects Test

The test to determine the effect of the presence of the model on turbulence measurements was performed in the University of Illinois laboratory. This test was performed in a 3×4 foot low-speed, low-turbulence tunnel. The model used was a 21-inch chord NACA 0012. In order to generate increased freestream turbulence levels of approximately 0.5% and 1.0% similar to those present in the IRT, turbulence generating grids were installed in the test section 30 inches upstream of the model leading edge. These are the same screens used by Lee[25] and Bragg et al.[7] The actual hot-wire mounting apparatus used in the IRT, which will be describe in more detail later, could not be

mounted to the fiberglass model. Therefore, a traverse system was used to position the probe at locations available with the IRT mounting apparatus. This corresponds to approximately 0.5 to 6 inches above the model surface at the 85% chord location. For a more complete description of the test section setup and traverse system, see Kerho.[26]

In order to keep the size of the test matrix reasonable, nearly all of the data were taken at a velocity of 100 mph, since this was the velocity at which most of the icing tunnel data were acquired. The majority of the data acquired for this test were taken at 10 kHz for 3 seconds. Six, three second sets were acquired at each condition. The low-pass filter on the anemometer was set at 5 kHz with a 3 Hz high pass filter used to remove the DC component and the influence of low-frequency velocity oscillations. Tests were also performed with a boundary layer trip near the leading edge of the model. The trip consisted of 0.012 inch beads sparsely scattered on a 0.25 inch wide piece of double-sided adhesive tape. The trailing edge of the trip was placed at the 5% chord location. Table 1 gives the conditions tested at each probe location and angle of attack.

Conditions 3, 4, and 5 in Table 1 were tested only at 8° angle of attack since this was where most of the IRT data were taken. For the same reason, additional measurements at varying velocities and filter settings were also taken at 8° angle of attack with the probe at 1.5 inches from the model.

Icing Research Tunnel Tests

As mentioned earlier, testing in the IRT was performed on two separate occasions. The first test involved shielding the hot-wire sensor by placing it above an airfoil at angle of attack. Figure 3 is a schematic drawing of the probe support used to position the sensor. The distance of the sensor from the model surface was adjustable from 0.5 to 6 inches in 0.5 inch increments by removing and replacing different size spacers above and below the probe. This entire fixture was bolted to the lower surface of a 21" chord, NACA 0012 model as shown.

With the tunnel velocity set at 100 and 250 mph, the model at 0° angle of attack, and the probe 6 inches from the surface to place the probe in the freestream flow, measurements were taken with nozzle air pressures (no water) varying from 0 to 80 psig. The probe was then moved to 1.5 inches from the surface. At a velocity of 100 mph, data were acquired at angles of attack of 4, 6, and 8° to assess the effects of model angle of attack. A set of data with varying nozzle air pressure but no water present was also acquired with the probe 1.5 inches from the model at 8° angle of attack and 100 mph. Air pressures of 0, 10, 30, and 50 psig were used.

For the measurements taken in the presence of the spray cloud, a data acquisition rate of 100 kHz was chosen in order to make sure that high-frequency droplet strikes could be resolved. Unless otherwise noted, the model was at 8° angle of attack, and the probe was 1.5 inches from the model surface. A small set of data was taken at temperatures below freezing to assess the usefulness of this technique in flight icing conditions.

In order to investigate the effects of MVD and LWC on the turbulence intensity level, data were acquired at the conditions summarized in Table 2. As noted, data were also acquired with only the nozzle air operating, and no water present at each condition. In a similar manner, the dependence of turbulence intensity on nozzle air and water pressure was investigated as summarized in Table 3. The effectiveness of the model shielding was checked at the 100 mph, MVD = 30 μm, LWC = 1.5 case by decreasing the angle of attack to 6, 4, and 0°.

A speed of 100 mph, droplet size of 20 microns, and LWC of 0.7 g/m^3 were chosen for testing the operation of the hot wire while ice was forming. Total temperatures of 25, 20, 15, and 10° F were tested. Several data sets were taken at each condition, until the ice accretion prevented the anemometer from functioning properly.

In the second test, no model was used, but two wires were operated simultaneously in an attempt to measure temperature fluctuations. This attempt was unsuccessful, therefore those results are not presented here. For details of this method, see Henze.[22] As this was a one day test, all data were taken at 100 mph. To facilitate the investigation of the possible temperature fluctuations data were acquired with no water present at nozzle air pressures varying from 0 to 80 psig. With the goals of supplementing the data set from the previous test, and assessing the need for shielding the sensor with a model in mind, a set of data was acquired in the water cloud without heating the nozzle air. Relatively low liquid water content levels were chosen, since that is where the droplet filtering methods had worked best previously. The cloud conditions chosen are summarized in Table 4.

Uncertainty Analysis

An analysis of the uncertainty in the measured quantities, the details of which are given in Henze,[22] was performed based on the general uncertainty analysis presented by Kline and Mclintock[27] and Coleman and Steele.[28] The uncertainty due to bias errors in the velocities measured in the IRT was found to be approximately 4 ft/s at conditions typical of those encountered during testing. The fact that the mean velocities measured by the hot-wire sensors were lower than those measured by the pitot probes in the IRT raised some concern about the accuracy of the resulting turbulence measurements. However, the turbulence intensity measurements were found to agree well with those estimated by a King's law analysis which relied only on the hot-wire voltages, and not the velocity calibration of the sensor. It was also determined through a statistical

analysis that a considerable amount of data could be removed by the droplet filtering techniques, and the turbulence intensity calculated from the remaining data would still be valid.

Results and Discussion

Effect of Model Shielding

The effect of the presence of the model on the turbulence intensity readings was investigated in the University of Illinois tunnel by positioning the probe relative to the model using the traverse system. The model angle of attack was varied from 0 to 12°, and the distance of the probe from the model surface ranged from 0.5 to 6 inches (the same range of locations which was available using the IRT mounting system).

The results obtained from moving the hot-wire sensor progressively closer to the model at 8° angle of attack are shown in Fig. 4 where turbulence intensity is plotted as a function of distance from the model. Data at all three turbulence intensity levels, and with and without a boundary layer trip are plotted. The boundary layer trip had no observable effect on the turbulence intensity measurements. The fact that the probe was inside the boundary layer at 0.5 inches was indicated by the large increase in turbulence level shown in Fig. 4 for all cases. The turbulence levels at each location and condition are given in Table 5 along with the change in turbulence intensity from 6 to 1.5 inches. Outside of the boundary layer a very slight increase in turbulence was observed as the probe approached the surface. For the lower freestream turbulence levels (clean tunnel and 0.5% grid) the increase in turbulence apparent at one inch was also likely due to the influence of the model boundary layer. With no grid present, the turbulence level increased from 0.15% at 6 inches to 0.25% at 1.5 inches (average of values with and without the boundary layer trip), an increase of 0.1%. With the 0.5% grid installed, the turbulence intensity 6 inches from the model averaged 0.56%, and only increased to 0.59% at 1.5 inches. Similarly, the difference in turbulence from 6 to 1.5 inches when the 1% grid was installed was just 0.06% from 0.99% to 1.05%.

It was apparent that the increase in turbulence intensity was larger when the freestream turbulence was low. This radiation of turbulence from the boundary layer added like the sum of the squares and therefore has a smaller contribution to the total when the freestream turbulence was high.

Fig. 5 shows the variation in turbulence level as the model angle of attack was increased with the probe at 1.5 inches from the model. Results with and without the 0.5% turbulence generating grid in the University of Illinois tunnel, and with and without nozzle air on in the IRT are shown for comparison. While there was a clear trend of increased turbulence with increasing angle of attack, it was difficult to quantify the effect of angle attack due to the amount of scatter in these data. However, at angles of 10° or less, the increase due to model angle of attack was quite small. These results all indicated that with the model at 10° angle of attack or less, and with the probe at least 1.5 inches from the model surface, the model had only a slight influence on the turbulence measurements. With the model at 8° angle of attack, and the probe 1.5 inches from the surface, as it was for most of the data taken in the IRT, this increase should be 0.05% or less at the freestream turbulence levels typical of the IRT.

Effectiveness of Sensor Shielding

It was obvious in initial tests that a considerable number of droplets were still striking the sensor even with the wire at 1.5 inches from the model surface, and the model at 8° angle of attack. With the probe at 1.5 inches from the surface, it could not be moved closer to the model without risking significantly increased turbulence measurements due to the boundary layer. Therefore, the model angle of attack was increased to 10°. This appeared to have no significant effect on the number of droplets striking the wire, so attempts were made to increase the momentum of the droplets, and thus there distance from the model by increasing the droplet size and tunnel velocity. Again, no significant change was observed. It was likely that smaller droplets in the cloud were passing close to the model, and/or droplets were being swept closer to the model by turbulent fluctuations.

Despite the fact that numerous droplets were still striking the sensor, the model was apparently serving to shield the probe to some extent. Figure 6 shows the results of varying the model angle of attack in cloud conditions. The standard deviation of the velocity, plotted here as a function of model angle of attack, was calculated using all of the data from each set without removing droplet strikes. The significant decrease in standard deviation with increasing angle of attack indicated that the model was indeed shielding the sensor.

The shielding effect of the model was also apparent in ice accretions on the probe support during the tests where the temperature was below freezing. Figure 7 is a photograph of the probe and its mounting support (see Fig. 3 for a diagram of this mounting apparatus) from above with ice accreted on the leading edge of the airfoil shaped support. It was apparent from the decreased ice accretion near the model that a significant amount of water was being deflected away from the model surface.

Despite the evidence that the model was indeed shielding the sensor from some of the droplets, this was not immediately apparent in the filtering results. Neither the percentage of data removed by the filter, nor the number of droplets detected, was observed to decrease significantly with increasing model angle of attack. (The droplet filtering and counting techniques will be explained in detail in the next section.) One possible explanation for

this observation is that the number of small droplets striking the wire was much higher in comparison to the number of large droplets being deflected by the model. Thus, no noticeable decrease in the number of droplets striking the wire was apparent as the model angle of attack increased.

In support of this theory, droplet size distribution data from Papadakis[29] et al. for an MVD of 22.6 microns was examined to determine the number of very small droplets present in a cloud relative to those at the MVD and larger. These data were given as the percentage of the total liquid water comprised of droplets of a given diameter, and are plotted in Fig. 8a. Figure 8b shows the distribution of the number of droplets in the cloud at a particular size calculated from these same data. It is important to note that these numbers are per cubic centimeter of total water, not air as is the case with LWC measurements. This analysis revealed that the droplet cloud contained significantly more very small droplets than droplets at the MVD and larger.

Assuming that larger droplets caused larger spikes in the data allowed an analysis of the size distribution of the droplets striking the wire. Larger voltage spikes were observed at lower angles of attack indicating that larger droplets were striking the wire. However, there were far more droplets spikes in the data with relatively small voltage peaks. This indicated that the number of very small droplets striking the wire was large compared to the number of larger droplets.

The duration of the droplet spikes was observed to be relatively constant regardless of the amplitude of the spike. Thus, a nearly constant number of data points were removed due to each spike. Therefore, because the number of droplets striking the wire was not varying significantly with model angle of attack, neither was the amount of data removed by the droplet filter. However, as the angle of attack was decreased, larger droplets were reaching the sensor resulting in larger spikes. These larger spikes were causing increased signal rms while not significantly increasing the number of droplet strikes counted or the percentage of data removed. The decreased ice accretion observed near the model was due to the fact that, as indicated by the droplet distribution in Fig. 8a, the deflected large droplets contained a large fraction of the liquid water in the cloud.

These observations made the need for the model shielding questionable. Therefore, as stated previously, data in the second IRT test were taken with no model present. It appears that at lower liquid water content levels, the model shielding may have been more effective than at the relatively high (1.5 g/m^3) LWC condition examined by the angle of attack sweep performed in the droplet cloud. This was indicated by the fact that a large percentage of data had to be removed even at very low water contents when the model was not present. With the model shielding, significantly less data were removed at these low LWCs. Unfortunately, the angle of attack sweep at a fairly high liquid water content was the only one performed in cloud conditions. The effectiveness of the model shielding could have been more clearly determined if similar data had been taken in various cloud conditions.

Droplet Filtering Technique

An acceleration threshold method was developed for identifying the droplet strikes in the hot-wire data. The term "threshold method" refers to removing data which exceed some preset level in a measured or derived quantity. The following explanation of this filtering method will rely on the time traces of velocity and acceleration data shown in Figs. 9 and 10. It is important to note that the calculated velocities and accelerations presented in these plots were not actual velocities or accelerations when a droplet struck the wire, but are the acceleration or velocity calculated based on the hot-wire calibration in air - not in water. The high heat transfer due to the water leads to unrealistically large "sensed" velocities and accelerations which can be removed using a threshold filter. The freestream velocity for these time traces was approximately 100 mph in a droplet cloud of MVD = 30 microns and LWC = 1.5 g/cm^3. The model angle of attack was set at 8°, and the sensor was 1.5 inches from the model surface. Time traces for the same conditions with no water present were also plotted for comparison. Figure 9 is a 0.01 second time trace, while Fig. 10 is a plot of a 0.002 second segment of the same data. The importance of using an acceleration threshold filter as opposed to a velocity threshold, as noted by Farrar et al.[20] in their work in bubbly flows, was apparent in these time traces. While the larger spikes due to droplets were clearly apparent in the velocity plots, some of the smaller spikes, apparently due to small drops or partial droplet strikes, were difficult to differentiate from freestream turbulence. Plotting the accelerations made even the smaller spikes considerably more apparent, and thus much easier to filter using a threshold method.

The acceleration threshold filtering method used is illustrated in Fig. 11. An upper and lower threshold, indicated by the two horizontal lines, was set just above the maximum absolute acceleration of a corresponding data set with the nozzle air operating at the appropriate pressure, but no water present. At 100 mph, a threshold level of 100,000 ft/s^2 was found to be appropriate for nearly all cases. When any acceleration value exceeded the threshold, it was considered to be part of a spike indicating droplet impingement. That point along with all points 0.0001 seconds (10 points in the case of data acquired at 100 kHz) before and after it were then marked to be excluded from turbulence intensity calculations. These additional points were removed to avoid the remaining "stumps" of the droplets spikes noted by Hetsroni, Cutler, and Sokolov.[16] Dotted lines were used to indicated the excluded points in Fig. 11. With the data

filtering complete, the turbulence intensity calculation was then performed on the remaining data. It can also be seen in this plot that some small spikes apparently indicating small droplet strikes fell below the threshold and were not filtered. However, in general the acceleration peaks caused by the droplets were much larger than those due to turbulent fluctuations in the air. As an indication that this was the case, for the data from which the time traces in Figs. 9 and 10 were extracted, the magnitude of the maximum acceleration in the no-water case was around $8x10^4$ ft/s^2, while the maximum sensed acceleration in the water-on case was much higher at almost $1x10^7$ ft/s^2. The data taken at 250 mph was not successfully filtered because the rate of droplet strikes was too high relative to the data acquisition rate.

There was some initial concern that setting such a threshold would essentially set the turbulence intensity by removing not only droplet strikes but any additional fluctuations caused by the presence of the water droplets which were not due to the water striking the wire. However, while the maximum acceleration in the water-off data plotted in Figs. 9 and 10, was 80,600 ft/s^2, applying a threshold level as low as 50,000 ft/s^2 to these data only removed 0.617% of the data reducing the turbulence intensity to 0.662% from 0.663%. This indicated that the majority of the accelerations in the water-off data were actually considerably lower than the maximum acceleration and thus considerably lower than the threshold level. Examining histograms of accelerations also revealed this type of distribution as shown in Fig. 12. This histogram was developed by dividing the total range of accelerations into "bins" and counting the number of measurements that fell into each. For this water-off case with a nozzle air pressure of 15 psig, the largest accelerations were found to be about 150,000 ft/s^2, therefore a threshold of 200,000 ft/s^2 was used to filter the corresponding water-on data sets. As shown in Fig. 12, the vast majority of accelerations were small compared to the maximum acceleration. If we make the assumption that any accelerations caused by the spray cloud which weren't due to droplets striking the wire were on the order of the accelerations in the water-off data, then the large majority of those accelerations were also well below the threshold.

The results of applying this filtering technique are shown in Fig. 13. This figure shows the results of applying the filter to the same data from which the time traces (Figs. 9-11) were extracted. The resulting turbulence intensity as the filter threshold was decreased were plotted here, along with the percent of the data removed by each filter setting. The turbulence level of the corresponding water-off data set was also plotted for reference. The turbulence intensity level was observed to approach that of the corresponding water-off case as the filter threshold decreased. The threshold level used to find the final droplet-filtered turbulence intensity in this case was 100,000 ft/s^2 which was found to be an appropriate filter threshold for the majority of the data taken at 100 mph. The decrease in turbulence intensity at levels below this was quite small indicating that most of the droplet strikes had been removed, but that the threshold was not so low that it was removing a considerable number of fluctuations which were not due to droplet strikes. The maximum acceleration in the water-off data was also indicated in Fig. 13. In this case, it appeared that some small droplets still circulating in the tunnel caused a few small spikes in the water-off data. Applying a 100,000 ft/s^2 threshold filter to this water-off data only removed 2 droplet strikes from the 1 second data set, which accounted for 0.047% of the data and resulted in a drop of 0.001% in turbulence intensity. Therefore, a threshold of 100,000 ft/s^2 was still considered appropriate in this case and others like it.

The amount of data removed from the water-on data set in Fig. 13, approximately 77% at a threshold level of 100,000 ft/s^2, was quite large. However, with the model shield present, applying the filter to data sets where the LWC was lower resulted in far less data being removed. Figure 14 is for the same conditions as Fig. 13 except that the LWC was 0.9 g/m^3 instead of 1.5 g/m^3. In this case only about 12% of the data were removed by a threshold of 100,000 ft/s^2.

IRT Turbulence Variations Due to Cloud Conditions

The effect of the variation of nozzle air pressure on the tunnel turbulence intensity level was examined in both IRT tests by acquiring data at varying nozzle air pressures with no water present. The results of the tests are shown in Fig. 15. The data marked with open symbols and connected by solid lines are those taken at 10 kHz with 5 kHz low-pass and 0.1 Hz high-pass filters. All of these measurements were taken in the free stream with no shielding. In the first test the model was present, however, it was at 0° angle of attack, and the probe was six inches from the surface. The solid circles are the results of various water-off data sets taken at 100 kHz with the model at 8° angle of attack and the probe at 1.5 inches from the model throughout the data acquisition period in the first test. Additional high-frequency oscillations passed by a higher low-pass filter used at higher acquisition rates, along with the increase due to the model shield, may explain why these turbulence measurements were generally higher than those taken at 10 kHz. The solid triangles represent the data acquired at 50 kHz from each of the two wires in the second IRT test. These data were reduced using the standard single-wire data reduction techniques for each wire, and the two resulting turbulence levels were averaged. These measurements were in reasonable agreement with the 10 kHz data.

The cause of the overall increase in the measured turbulence intensities observed in the second test as opposed to those from the first is not clear at this time. A new tunnel spray bar system was installed in the IRT

between these tests. However, it uses the same nozzles, and was designed to reduce the turbulence level. It is likely that there were considerable spatial variations in the turbulence level throughout the IRT test section due to the presence of the spray bars and nozzles. This was probably the cause of the observed difference since the sensor was in different locations for the two tests.

Overall, these water-off turbulence measurements agreed reasonably with those of other researchers. Poinsatte[3] found turbulence levels of 0.6%, 0.52%, and 0.7% at velocities of 70, 140, and 210 mph respectively with no nozzle air pressure. Gonsalez[2] also measured turbulence intensity levels which increased with nozzle air pressure and tunnel velocity. At 100 mph, he found a clean tunnel turbulence level of approximately 0.6% increasing to about 1.1% with the nozzle air pressure at 80 psig. These measurements agreed very well with the data from the second IRT test (with the nozzle air heated) where the corresponding turbulence levels were 0.58% with the nozzle air off and 1.06% at 80 psig nozzle air pressure. All of these data are plotted in Fig. 16 along with the two corresponding water-off data points from the current test.

It was apparent that increasing nozzle air pressure caused a significant increase in the tunnel freestream turbulence level. This was not surprising, as the air from the nozzles entered the free stream with a considerable cross-flow component. Small, low-pressure jets (5 psig.) directed upwind were used to increase turbulence in a wind tunnel to levels up to 0.25%.[30] Thus it was a logical conclusion that the cross flow component of the IRT nozzle jets at high pressures would cause increased turbulence. Frequency spectrums of the hot-wire voltage with the nozzle air off and at 80 psig were compared as shown in Fig. 17. This comparison indicated that at frequencies below 1000 Hz, the increase in turbulence intensity due to nozzle air was a broad band increase - not an increase in fluctuations in any specific range of frequencies.

The effect of nozzle water pressure on turbulence level was explored in both of the two IRT tests by taking measurements at varying nozzle water pressures for a given air pressure. The results are shown in Fig. 18 where turbulence intensity levels at constant nozzle air pressures are plotted as a function of nozzle water pressure. Again an overall increase in turbulence level with increased nozzle air pressure was seen, and the measurements from the second test (no model) showed higher turbulence at a given air pressure. Unfortunately, all of these data were acquired at relatively high LWCs or without the model. As noted earlier, large amounts of data were removed in these conditions. This was likely the reason for the scatter in the data. There was an apparent increase in turbulence with water pressure seen in the two 30 psig nozzle air and 15 psig nozzle air, no model case. An increase in the number of small or partial droplet strikes missed by the filtering method was probably responsible for this trend and may have also been contributing to the scatter in all of these data. However, in each of the other three cases the nozzle water pressure had little effect on the turbulence intensity. The effects of air and water pressure will be addressed more thoroughly later in this section.

In the first IRT test turbulence intensity data were taken throughout the droplet size and water content range of the IRT. These results are presented in Fig. 19. Water-off cases at the same nozzle air pressures were plotted for comparison. The general trend which emerged was an increase in turbulence intensity as droplet size decreased and liquid water content increased. This agreed with earlier observations since an increase in air pressure caused a decrease in droplet size, and as water pressure was increased to increase LWC, nozzle air pressure must also increase to maintain a given droplet size. Based on this, it was apparent that this turbulence trend was primarily due to higher nozzle air pressures at higher LWCs and lower MVDs. In general, the turbulence intensities calculated after filtering water droplets from the spray-on cases were slightly higher than those from water-off data. This could have been partially due to water droplet interactions with the freestream flow, but was again likely due to small spikes in the hot-wire signal due to small droplets or partial droplet strikes which fell below the filter threshold as was observed in Fig. 11.

Due to the scatter in the data at specific air and water pressures (Fig. 18), the exact influence of nozzle water pressure was not clear. Thus, further analysis of the data was performed in order to provide more evidence that the nozzle air pressure was the primary cause of the observed increase in turbulence. A multi-variable linear regression performed on the water-on data from the first IRT test resulted in the following equation for the turbulence intensity as a function of nozzle air and water pressure.

$$TI = 0.522 + 0.00613 \times P_{air} + 0.000145 \times P_{water} \quad (6)$$

The coefficient on the air pressure term is over 40 times that of the water pressure term, again indicating that turbulence intensity was largely a function of air pressure. For 95% confidence in this case, the critical t value was 1.701. The observed t values for air and water pressure were 10.24 and 1.343 respectively. The fact that the t value for air pressure was considerably higher than the critical value indicates that air pressure was an important factor in determining turbulence intensity, while the t value for water pressure was lower than the critical value indicated that water pressure was not important.

Effect of Heated Nozzle Air on Turbulence Measurements

As noted earlier, the air exiting the IRT spray nozzles was heated to approximately 180° F to prevent ice from

forming in the nozzles. It was likely that this hot air was causing high-frequency temperature fluctuations which were being misinterpreted as velocity fluctuations and thus contributing to the measured turbulence intensity values.

In order to examine and quantify this effect, identical turbulence measurements were taken at varying nozzle air pressures, with and without the nozzle air heated. The results of these measurements are plotted in Fig. 20. As expected, the heating of the nozzle air did cause an increase in the turbulence intensity readings, apparently due to increased temperature fluctuations increasing the fluctuation in the heat transfer from the wire. The measurements taken with no nozzle air pressure prior to both the heated and cool air data acquisition matched very well at values of 0.58% and 0.584%. At 20 psig air pressure, the increase due to the heated nozzle air was 0.037%, from 0.725% to 0.762% while at 80 psig the heated air caused the turbulence intensity to increase from 0.991% to 1.063%, an increase of 0.072%. This larger increase at higher nozzle air pressures indicated that as more heated air was introduced into the freestream flow by the nozzles, the temperature fluctuations seen in the test section increased.

Based on an analysis from TSI Technical Bulletin 16,[24] turbulence intensity values due to different sources can be combined as the square root of the sum of the squares. Thus, the error in the turbulence intensity due to the temperature fluctuation, $TI_{T_{rms}}$, can be found using equation (7).

$$TI_{T_{rms}} = \sqrt{(TI_{hot})^2 - (TI_{cool})^2} \qquad (7)$$

TI_{hot} and TI_{cool} are the turbulence intensities with and without the nozzle air heated, respectively. The standard deviation of the temperature, T_{rms}, was then found using equation (8) which is also based on the analysis in the TSI bulletin.

$$T_{rms} = \frac{TI_{T_{rms}}}{200}(T_w - T_a) \qquad (8)$$

T_w and T_a are the wire operating temperature and the ambient temperature. The calculated standard deviations are given in Table 6. These fluctuations were found to be quite small (0.34 °C maximum) and, as expected, were observed to increase with increasing nozzle air pressure.

It is also quite likely that these temperature fluctuations are spatially dependent on location relative to a nozzle. Therefore, it is likely that this effect is dependent on location in the tunnel test section. However, this spatial variation was not studied in this test.

Turbulence Intensity Measurements in Icing Conditions

While all of the testing discussed to this point was performed at temperatures near room temperature, a set of data was acquired in icing conditions to assess the suitability of these experimental methods for use in flight test icing conditions. Turbulence measurements were taken until the ice accretion prevented the sensor from operating properly. Surprisingly, the ice accretion did not lead to sensor wire breakage. Close-up inspection of the ice formations revealed that the ice growing on the wire supports eventually became thick enough to block the wire from the freestream flow, but the heat of the wire kept a small area around the wire clear of ice. The turbulence intensity level of the droplet filtered data became unpredictable soon after ice began to accrete. However, several of the data sets taken 1 minute or less after the cloud was turned on were successfully filtered to give a tunnel turbulence level near that of the water off cases. This test indicated that the droplet filtering technique could be successfully employed in icing conditions if the probe could be shielded from ice accretion until immediately before measurements were taken, or if the probe could be effectively anti-iced or periodically de-iced.

Conclusions

As part of this research, a successful method for measuring turbulence intensity in icing cloud conditions was developed. Based on this development process, the following conclusions can be made.

1. A high data acquisition rate was found to be necessary for resolving droplet strikes in the hot-wire data. Data in the first test were acquired at 100 kHz which was found to be more than adequate for resolving the droplet strikes at 100 mph. A portion of the 100 mph data acquired in the second test was acquired at 50 kHz and was also successfully filtered. However, at 250 mph, the data could not be successfully filtered, because the frequency of droplets striking the sensor was too high relative to the data acquisition rate.
2. The use of an acceleration threshold as opposed to a velocity threshold was critical in identifying small or partial droplet strikes which resulted in smaller amplitude spikes in the hot-wire data.
3. The use of an airfoil to shield the sensor resulted in slight increases in the measured turbulence intensity. With the probe at 1.5 inches from the model surface and the model at 8° angle of attack, this increase was at most 0.06% at turbulence intensity levels typical of those in the IRT.
4. With some modification, the method could be used effectively in conditions at temperatures below freezing where ice was accreting.

The droplet filtering technique was used to measure turbulence intensity in the IRT spray cloud. The following conclusions were reached based on these measurements.

1. Turbulence intensity was found to increase significantly as nozzle air pressure increased. With

nozzle air pressure increasing from 0 to 80 psig, the freestream turbulence level increased from approximately 0.6% to 1.0%.

2. Nozzle water pressure had little if any effect on turbulence intensity. Slight increases with increasing water pressure were likely due to an increase in the number of small droplet strikes missed by the droplet filter at higher LWCs.
3. Turbulence intensity in the spray cloud was found to increase with increasing LWC and decreasing drop size. These trends were again attributable to increased air pressure.
4. Nozzle air, which was heated to prevent ice buildup in the nozzles, did cause temperature fluctuations which resulted in artificially high turbulence measurements. These temperature fluctuations increased with increasing nozzle air pressure. At the highest nozzle air pressure of 80 psig, the temperature fluctuation was found to be 0.33 °C, and caused an increase of 0.07% in turbulence intensity from 0.99% to 1.06%.
5. Small increases in turbulence intensity were observed when water droplets were present over the turbulence intensity at a given nozzle air pressure with the water off (for example, .015% increase at 100 psig water pressure). It was not possible to distinguish whether this small increase in turbulence was caused by the presence of the droplets or from errors due to the filtering technique.

References

[1] Dryden, H.L., and Kuethe, A.M., "Effect of Turbulence in Wind Tunnel Measurements," NACA Report No. 342, 1930

[2] Gonsalez, J.C., NASA Lewis Research Center, Cleveland, Ohio, personal communication, June, 1996

[3] Poinsatte, P.E., "Heat Transfer Measurements From a NACA 0012 Airfoil in Flight and in the NASA Lewis Research Tunnel," NASA CR-4278, 1990

[4] Kuethe, A.M., and Chow, C.Y., *Foundations of Aerodynamics: Bases of Aerodynamic Design, Fourth Edition*, John Wiley and Sons, New York, 1986

[5] Tani, I., "Boundary layer Transition" *Annual Review of Fluid Mechanics*, Sears, W.R., Editor, VanDyke, M., Associate Editor 1969

[6] Green, J.E., "On the Influence of Freestream Turbulence on a Turbulent Boundary Layer, As it Relates to Wind Tunnel Testing at Subsonic Speeds," AGARD Report No.602, 1972

[7] Bragg, M. B., Cummings, M. J., Lee, S., and Henze, C. M., "Boundary Layer and heat Transfer Measurements on an Airfoil with Simulated Ice Roughness," AIAA Paper 96-0866, 34th Aerospace Sciences Meeting and Exhibit, Reno, NV 1996

[8] Junkhan, G.H., and Serovy, G.K., "Effects of freestream Turbulence and Pressure Gradient on Flat-Plate Boundary layer Velocity Profiles and Heat Transfer," *Journal of Heat Transfer*, May, 1967

[9] Blair, M.F., "Influence of Freestream Turbulence on Turbulent Boundary Layer Heat Transfer and Mean Profile Development, Part 1 - Experimental Data," *Journal of Heat Transfer*, Vol. 105, February, 1983

[10] VanFossen, G. J. Jr., and Simoneau, R. J., "A Study of the Relationship Between Freestream Turbulence and Stagnation Region Heat Transfer," *Journal of Heat Transfer*, Vol. 109, February, 1987

[11] VanFossen, G. J., Simoneau, R. J., Olsen, W.A. Jr., and Shaw, R. J., "Heat Transfer Distributions Around Nominal Ice Accretion Shapes Formed on a Cylinder in the NASA Lewis Icing Research Tunnel," AIAA Paper 84-0017, 22nd Aerospace Sciences Meeting, Reno, NV, 1984

[12] Gelder, T. F., and Lewis, J. P., "Comparison of Heat Transfer From Airfoil in Natural and Simulated Icing conditions," NACA TN-2480, September 1951

[13] Merceret, F.J., "An Experimental Study to Determine the Utility of Standard Commercial Hot-wire and Coated Wedge-Shaped Hot-film Probes for Measurement of Turbulence in Water-Contaminated Air Flows," Technical Report #40, Chesapeake Bay Institute, The John's Hopkins University, 1968

[14] Merceret, F.J., "An Experimental Study to Determine the Utility of Standard Commercial Hot-wire and Coated Wedge-Shaped Hot-film Probes for Measurement of Turbulence in Water-Contaminated Air Flows, Part II," Technical Report #40, Chesepeake Bay Institute, The John's Hopkins University, 1969

[15] Goldschmidt, V.W. and Householder, M.K., "The Hotwire Anemometer as an Aerosol Droplet Size Sampler," *Atmospheric Environment*,Vol. 3, Pergamon Press, 1969

[16] Hetsroni, G., Cutler, J.M., and Sokolov, "Measurements of Velocity and Droplets Concentration in Two-Phase Flows," *Journal of Applied Mechanics, Transactions of the ASME*, June 1969

[17] Hetsroni, G., and Sokolov, "Distribution of Mass, Velocity, and Intensity of Turbulence in a Two-Phase Turbulent Jet," *Journal of Applied Mechanics, Transactions of the ASME*, June 1971

[18] Bruun, H.H., *Hot-Wire Anemometry: Principles and Signal Analysis*, Oxford University Press, 1995

[19] Liu, T.J., and Bankoff, S.G., "Structure of Air -Water Bubbly Flow in a Vertical Pipe I. Liquid Mean Velocity and Turbulence Measurements," *International Journal of Heat and Mass Transfer*, Vol. 36, No. 4

[20] Farrar, B., Samways, A.L., Ali, J., and Bruun, H.H., "A computer-Based Hot-Film Technique for Two-Phase Flow Measurements," *Meas. Sci. Technol.* 6, 1995, pp. 1528-1537

[21] Ritsch, M.L. and Davidson, J.H., "Phase Discrimination in Gas-Particle Flows Using Thermal Anemometry," *Journal of Fluids Engineering, Transactions of the ASME*, Vol. 114, December, 1992

[22] Henze, C.M., "Turbulence Intensity Measurements in Icing Cloud Conditions, " M.S. Thesis, University of Illinois, 1997.

[23] Anon., "IFA 100 Intelligent Flow Analyzer System Instruction Manual," TSI incorporated, 1983

[24] Anon., "Temperature Compensation of Thermal Sensors," TSI Technical Bulletin 16

[25] Lee, S., "Heat Transfer On An Airfoil With Large Distributed Leading-Edge Roughness," M.S. Thesis, University of Illinois, 1997

[26] Kerho, M.F., "Effect of Distributed Roughness Near an Airfoil Leading Edge On Boundary layer Devlopment and Transition," Ph.D. Thesis, University of Illinois, 1995

[27] Kline, S.J., and McClintock, F.A., "Describing Uncertainties in Single-Sample Experiments," *Mechanical Engineering*, Jan., 1953

[28] Coleman, H.W., and Steele, W.G., Jr., *Experimentation and Uncertainty Analysis for Engineers*, John Wiley and Sons, Inc., New York, 1989

[29] Papadakis, M., Elangonan, R., Freund, G. A., Breer, M., Zumwalt, G. W., and Whitmer, L., "An Experimental Method for Measuring Water Droplet Impingement Efficiency on Two- and Three-Dimensional Bodies," NASA Contractor Report 4257, 1989

[30] Kendall, J.M., "Boundary Layer Receptivity to Freestream Turbulence," AIAA paper 90-1504, AIAA 21st Fluid Dynamics, Plasma Dynamics and Lasers Conference, Seattle, WA, June, 1990

Table 1. Matrix of test conditions for model shielding effects test

Test Conditions:
1 – no turbulence grid, no boundary-layer trip
2 – 0.5% turbulence grid, no boundary-layer trip
3 – boundary-layer trip, no turbulence grid
4 – 0.5% turbulence grid and boundary-layer trip
5 – 1% turbulence grid, no boundary-layer trip

Angle of Attack (degrees)	Distance from model surface (inches)							
	6	5	4	3	2	1.5	1	0.5
0	1,2	1	1,2	1	1,2	1,2	1,2	1,2
2	1,2	1	1,2	1	1,2	1,2	1,2	1,2
4	1,2	1	1,2	1	1,2	1,2	1,2	1,2
6	1,2		1,2		1,2	1,2	1,2	1,2
8	1,2,3,4,5	1,2	1,2,3,4,5	1,2	1,2,3,4,5	1,2,3,4,5	1,2,3,4,5	1,2,3,4,5
10	1,2		1,2		1,2	1,2	1,2	
12	1,2		1,2		1,2	1,2		

Table 2. Summary of IRT cloud conditions - varying LWC and MVD in the first IRT test.

Velocity (mph)	MVD (μm)	LWC (g/m^3)	Air Pressure	Water Pressure
100	20	0.7	11.03	31.12
	20	1.3	35.02	130.78
	20	1.9	70	318.34
	30	0.9	12.04	46.08
	30	1.5	28.06	147.89
	30	2	42.81	282.58
	40	0.9	10.67	43.58
	40	1.5	23.93	138.53
	40	2	35.92	264.2
250	20	0.4	13.41	40.3
	20	0.65	34.1	126.32
	20	0.9	60.52	268.14
	30	0.5	13.87	56.29
	30	0.75	27.41	142.91
	30	1	41.89	273.12
	40	0.5	12.17	53.06
	40	0.75	23.38	133.85
	40	1	35.22	255.49

Model angle of attack 8°, probe 1.5 inches from model surface. Data acquired at each air pressure with and without water on.

Table 3. Summary of cloud conditions - varying air and water pressures in the first IRT test

Velocity (mph)	MVD (μm)	LWC (g/m^3)	Air Pressure	Water Pressure
100			20	0
	18	0.91	20	60
	25	1.11	20	80
	35.5	1.29	20	100
			30	0
	13.5	0.74	30	60
	16	0.96	30	80
	18.5	1.14	30	100
			40	0
	12	0.58	40	60
	14	0.82	40	80
	15.5	1.01	40	100
250			20	0
	18	0.46	20	60
	25	0.56	20	80
	35.5	0.65	20	100
			30	0
	13.5	0.38	30	60
	16	0.49	30	80
	18.5	0.58	30	100
			40	0
	12	0.3	40	60
	14	0.42	40	80
	15.5	0.51	40	100

Model angle of attack 8°, probe location 1.5 inches from model surface. Data also acquired at each air pressure with no water present.

Table 4. Test conditions in second IRT test

MVD (μm)	LWC (g/m^3)	Air Pressure	Water Pressure
		10	0
17.5	0.55	10	20
23.6	0.78	10	30
		15	0
15.5	0.66	15	30
19	0.85	15	40
23.5	1.01	15	50
29	1.14	15	60
37	1.27	15	70
19	1.05	20	60
16.2	0.96	25	60
		30	0
15*	0.87	30	60
15.9	1.01	30	70
18	1.23	30	90
21*	1.42	30	110

Table 5. Turbulence intensity values at various distances from the model surface, and at various test conditions - Model at 8° angle of attack, and velocity approximately 100 mph. (*: condition repeated with nozzle air heated)

Test Conditions:
1 - no turbulence grid, no boundary-layer trip
2 - 0.5% turbulence grid, no boundary-layer trip
3 - boundary-layer trip, no grid
4 - 0.5% turbulence grid and boundary-layer trip
5 - 1% turbulence grid, no boundary-layer trip

distance from surface (in.)	condition				
	1	2	3	4	5
6	0.14	0.55	0.16	0.57	0.99
5	0.17	0.55	-	-	-
4	0.23	0.56	0.22	0.57	1
3	0.22	0.56	-	-	-
2	0.26	0.57	0.24	0.59	1.03
1.5	0.25	0.58	0.25	0.59	1.05
1	0.35	0.61	0.35	0.66	1.01
0.5	2.05	2.44	5.82	4.23	5.38
TI@1.5 - TI@6	0.11	0.03	0.09	0.02	0.06

Table 6. Standard deviation in temperature with nozzle air heated

Nozzle Air Pressure (psig)	Standard Deviation in Temperature (°C)
20	0.216092654
40	0.312274848
60	0.343202003
80	0.330482343

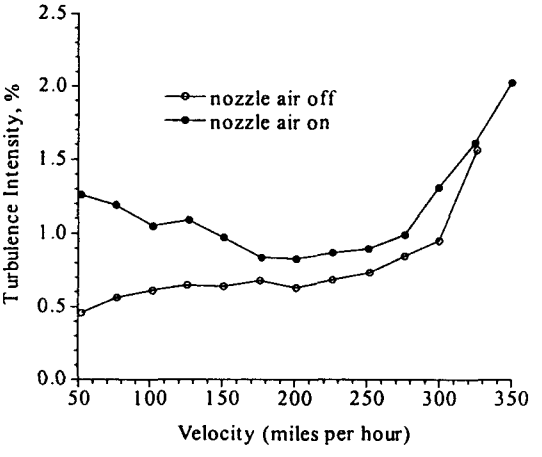

Figure 1. Turbulence Intensity as a function of velocity in the NASA Lewis Icing Research Tunnel (IRT) measured by Gonsalez[2]. Measurements taken without the nozzles operating (nozzle air off), and with nozzle air pressure at 80 psig with no water present (nozzle air on).

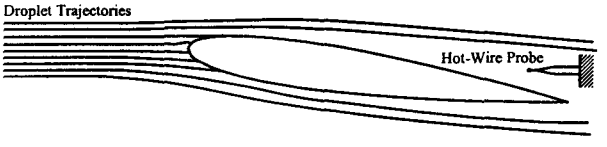

Figure 2. Droplet Trajectories over NACA 0012 airfoil. Hot-wire probe shielded by airfoil.

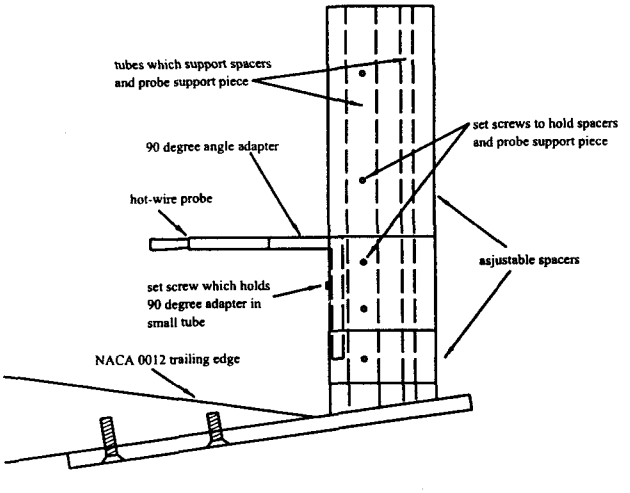

Figure 3. Hot-wire mounting apparatus used with 21" chord NACA 0012 model in the IRT

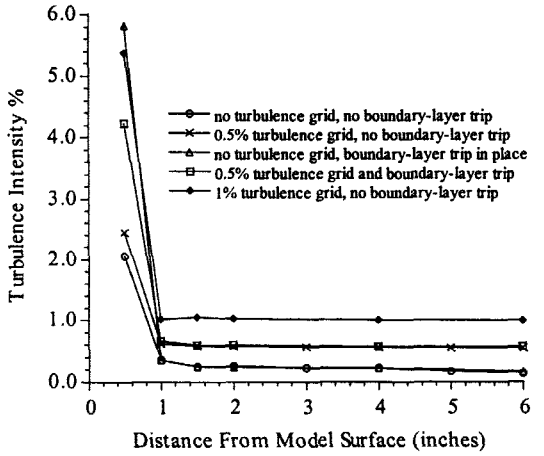

Figure 4. Turbulence intensity levels measured in the University of Illinois 3x4 foot tunnel as a function of distance from the model surface. 85% chord location, velocity = 100 mph, angle of attack=8°.

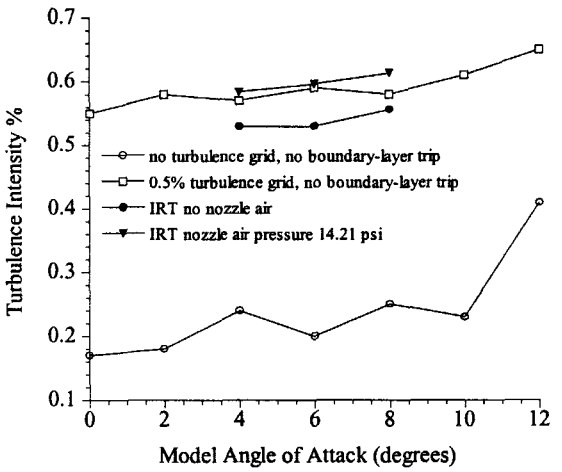

Figure 5. Variation in turbulence intensity with model angle of attack. Probe 1.5 inches from surface at 85% chord location. Velocity 100mph.

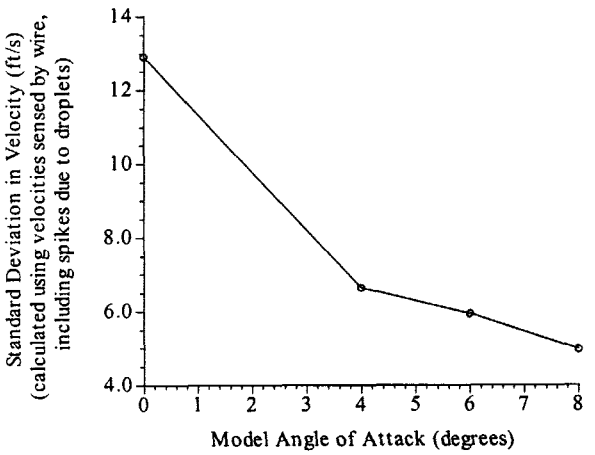

Figure 6. Standard deviation of velocity signal, including droplet strikes, at varying angle of attack in IRT spray cloud. Velocity 100mph, LWC = 1.5 g/m^3, MVD = μm.

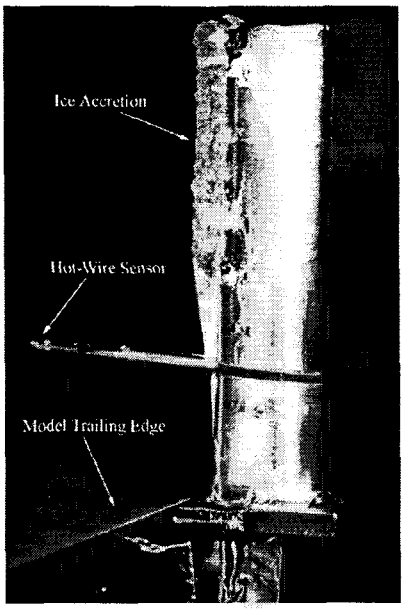

Figure 7. Ice accretion on hot-wire mounting support. Velocity = 100 mph, LWC = 0.7 g/m^3, MVD = 20μm, T_0 = 25 °F.

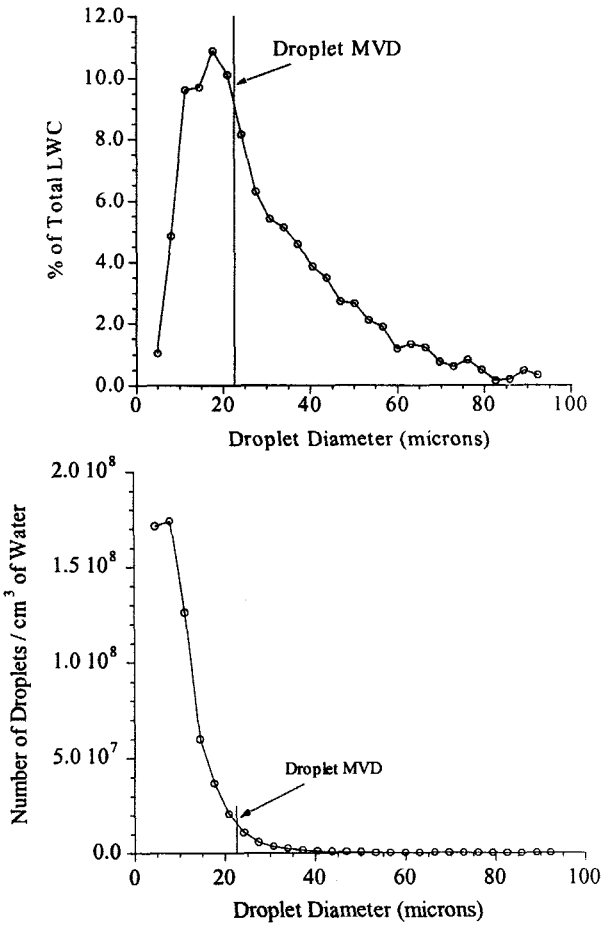

Figure 8. Droplet size distributions by % of total water, and number of droplets per cm^3. MVD = 22.6 μm. (Data from Papadakis et al.[29])

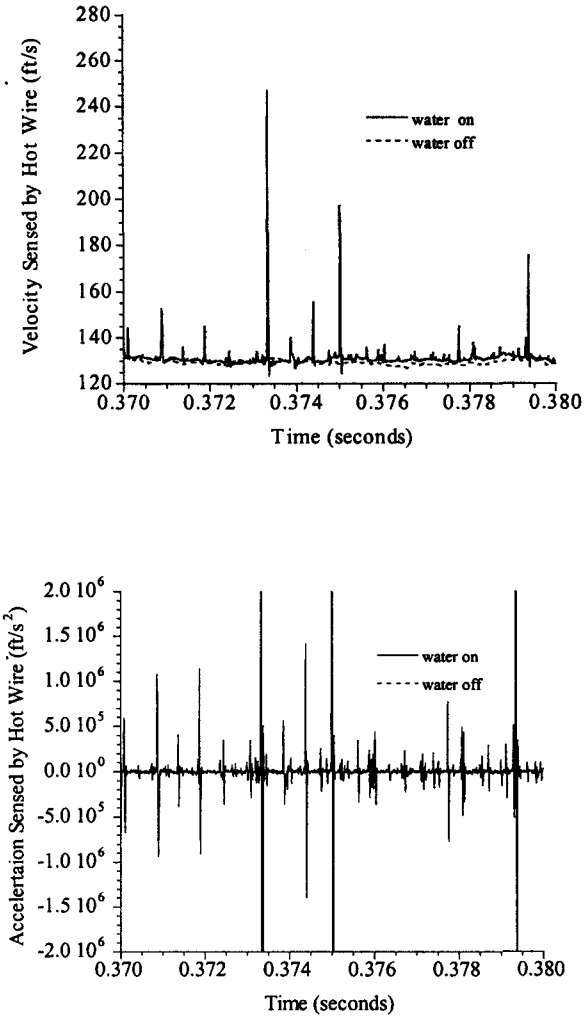

Figure 9. Velocity and acceleration time traces. MVD = 30 μm, LWC = 1.5 g/m^3, velocity = 100 mph.

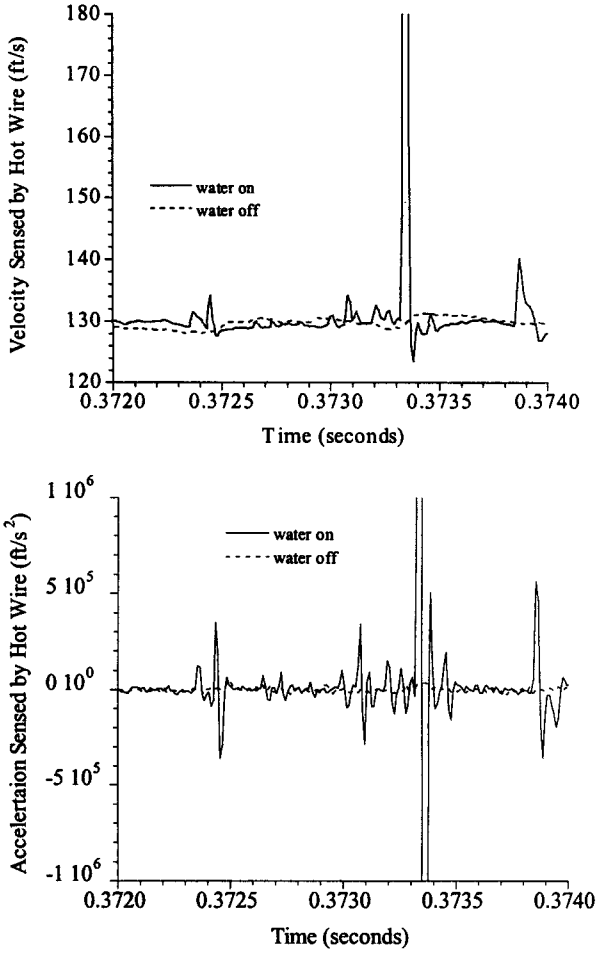

Figure 10. Shorter segments of the same time traces shown in Fig 9.

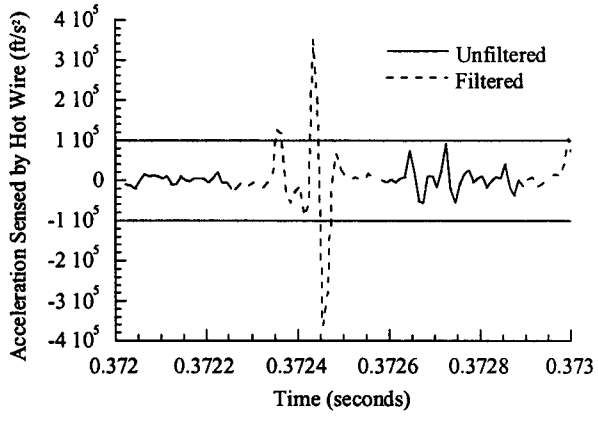

Figure 11. Illustration of droplet filtering technique applied to a segment of the data shown in the previous two figures. Horizontal lines indicate acceleration threshold. Dotted line indicates data removed by filter.

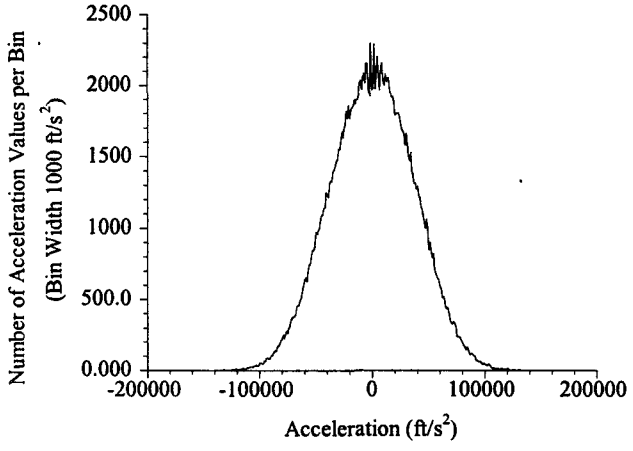

Figure 12. Histogram of accelerations in a water-off data set at 100 mph and 15 psig nozzle air pressure.

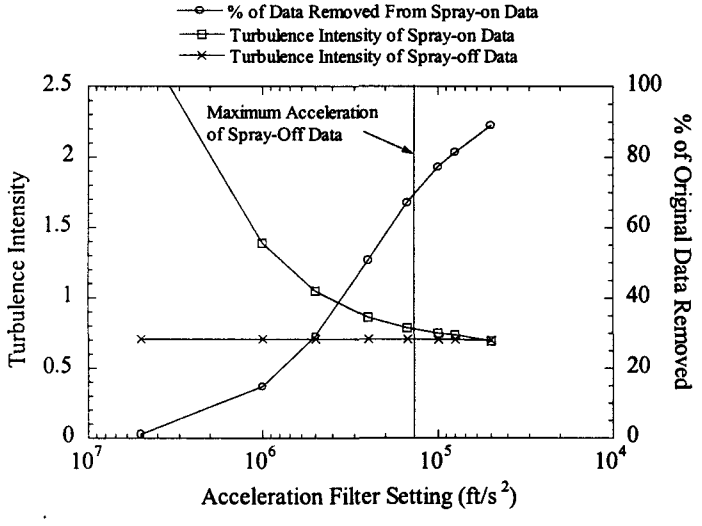

Figure 13. Turbulence intensity and percent of data removed as a function of acceleration threshold. Turbulence intensity and maximum acceleration of corresponding water-off data are plotted for reference. Same conditions as Figs. 9 and 10.

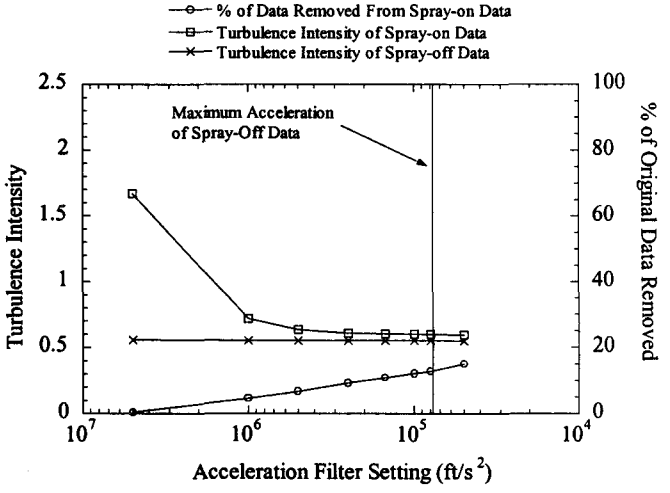

Figure 14. Turbulence intensity and percent of data removed as a function of acceleration threshold. T.I. and maximum acceleration of corresponding water-off data are plotted for reference. Same conditions as Fig. 13 with LWC reduced to 0.9 g/m^3.

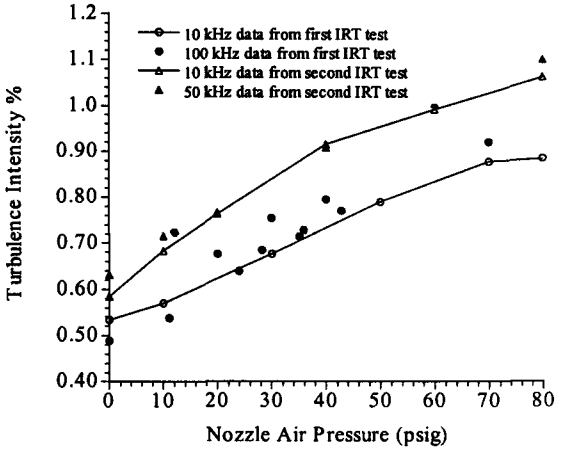

Figure 15. Turbulence intensity variation with nozzle air pressure at 100 mph. No water present.

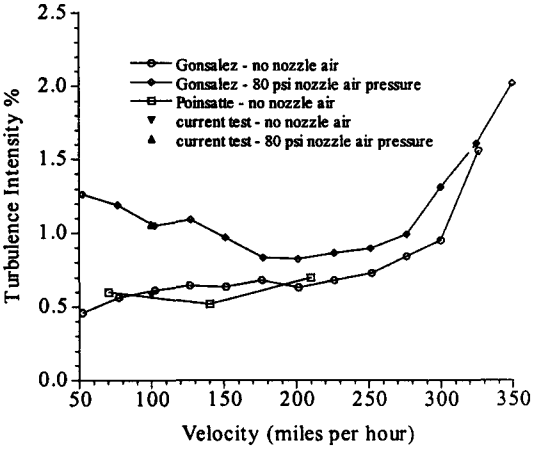

Figure 16. Turbulence intensity as a function of velocity from Poinsatte[3] and Gonsalez[2]. Two water off data points from the second IRT test included for comparison.

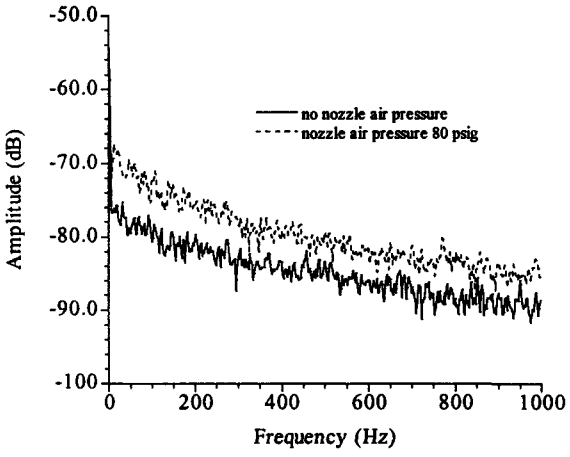

Figure 17. Frequency spectrums acquired from voltage signal in IRT with no nozzle air pressure and 80 psig nozzle air pressure (no water).

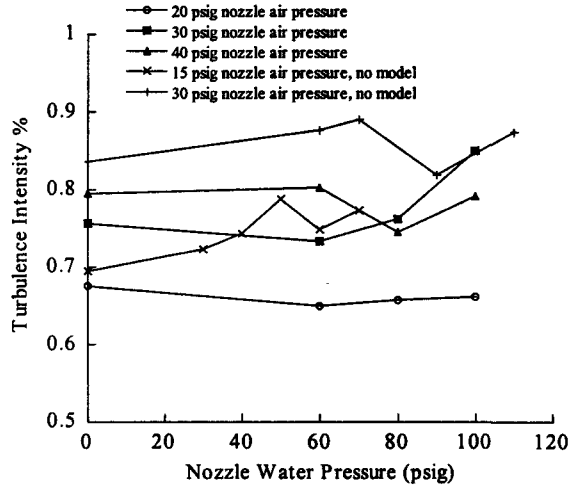

Figure 18. Turbulence intensity as a function of nozzle water pressure at various nozzle air pressures

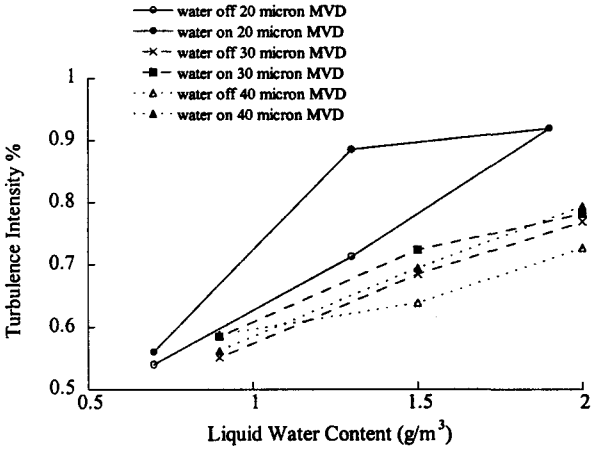

Figure 19. Turbulence intensity as a function of liquid water content at 3 droplet sizes. Filtered spray-on and corresponding spray-off cases plotted for comparison.

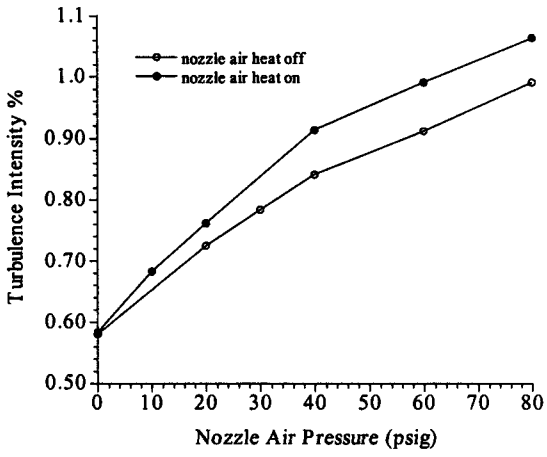

Figure 20. Turbulence intensity as a function of nozzle air pressure with and without nozzle air heated